Hierarchically Structured, Double-Periodic Inverse Composite Opals

Markus Retsch and Ulrich Jonas**

A versatile colloidal templating strategy to fabricate hierarchically structured inverse opals is investigated. A sequence of infiltration and pyrolysis steps provides access to a range of material combinations such as SiO_2, Al_2O_3, or TiO_2. The experimental results also document the feasibility of this method to fabricate porous polymer films with a double periodic pore lattice.

1. Introduction

Porous materials can be classified as contiguous networks, which consist of microporous (below 2 nm), mesoporous (2–50 nm), and macroporous (larger than 50 nm) channels and voids. Networks, which comprise various classes of pores with characteristically different dimensions, are termed "hierarchical". An important class of porous materials is given by so-called inverse opals, which are quite generally obtained by a colloidal crystal template. The crystalline order in combination with a periodic change of refractive index renders such materials suitable for applications relying on optical sensing[1,2] or waveguiding.[3] The porosity of inverse opals typically falls into the range of macropores. In combination with additional templating entities such as surfactants or block-copolymers, an additional, smaller level of porosity can be introduced into the inverse opal skeleton.[4] The resulting material represents a hierarchically structured porous film or monolith. Two of the key characteristics, which have been raising tremendous interest in hierarchically structured porous materials, are their large surface area and transport phenomena. The surface area is governed by the extent of nanostructuring of the smallest entities, which produces huge interfaces compared to non-structured bulk materials of the same volume. The presence of interconnected transport channels, which split into finer and finer subfeatures, severely affects transport processes and facilitates diffusion to the smallest structures. Diffusion measurements on monomodal inverse opals using fluorescence correlation spectroscopy (FCS) have revealed that increasing confinement of the probe particles, that is, in samples with smaller pores, results in a significant reduction of the diffusion coefficient.[5]

The combination of large surface area and hierarchical transport paths has sparked research to adapt these structures to a range of potential applications, such as catalysis,[6,7] or filtration.[8] For the purpose of catalysis, an efficient mass transport is ensured by interconnected macropores. This allows unconstrained diffusion of large molecules, like proteins, to the reaction or detection sites, which are commonly located in the meso- and micropores of such hierarchical materials. Due to this pore hierarchy, these materials possess a very large inner surface area, and can thus expose larger amounts of catalysts or receptors to the penetrating medium. Based on their importance, hierarchically porous materials and their preparation methods have been covered by several reviews.[9–13]

The actual fabrication of hierarchical networks can be achieved in various ways: quite commonly, colloid particles are used for templating the macropores, while meso- and micropores can be introduced by phase separation of block copolymers[14] or surfactants.[15]

The combination of colloidal templating and phase separation represents a bottom up approach to hierarchical materials. Also top down techniques were demonstrated, which apply material sculpturing techniques from macroscopic dimensions down to the micrometer scale. This was demonstrated by deposition within confined space,[14,16,17] plotting of discrete drops,[18] or by post-modification of a homogenous crystal.[19–21]

Whereas a lot of work has been devoted to the combination of macro-, meso-, and micropores, only little effort has been directed to the combination of various macropores in one material. As Wang et al. showed, the tetrahedral voids of a colloidal crystal could be filled with smaller particles in a single vertical deposition step, which resulted in a porous interconnected network with well-defined order after replication.[22,23] Combining small silica and large polystyrene spheres in a bimodal template, Chai et al. demonstrated the replication of these two particle length scales into a meso- and macroporous hierarchical carbon network.[24] Yan et al. used micromolding in an inverse opal structure to template monodisperse, mesoporous silica spheres with channels of 5 nm diameter.[25] Recently, Cho and Moon combined interference lithography and colloidal particle self-assembly to fabricate hierarchically structured TiO_2 films

Prof. M. Retsch
University of Bayreuth
Physical Chemistry–Polymer Systems
Universitätsstr. 30, 95447 Bayreuth, Germany
E-mail: markus.retsch@uni-bayreuth.de
Prof. U. Jonas
University of Siegen
Macromolecular Chemistry
Adolf-Reichwein-Strasse 2, 57076 Siegen, Germany
Foundation for Research and Technology - Hellas (FORTH)
Institute of Electronic Structure & Laser (IESL)
Bio-Organic Materials Chemistry Laboratory (BOMCLab)
Nikolaou Plastira 100, Vassilika Vouton,
P.O. Box 1527, 71110 Heraklion, Crete, Greece
E-mail: jonas@chemie.uni-siegen.de

DOI: 10.1002/adfm.201300803

for efficient dye-sensitized solar cells.[26,27] Furthermore, interfacial assembly techniques leading to hierarchical colloidal composites in thin films or even colloidal monolayers have been reported.[28–30] The aim of the work presented here is to close the 10–100 nm gap currently posed by conventional methods, which provide porous materials either with micropores (nanometer dimensions) or on a much larger micrometer scale.

The structural concept followed here is based on a hierarchy of colloidal crystal with high crystalline order (CC), amorphous (or less ordered) colloidal aggregates (CA), and inverse opal (iO) generations, which are built inside each other in successive steps. This architectural concept can be very generally represented as: generation *x* @ … @ generation 2 @ generation 1, where the higher generation forms a lattice structure inside the voids of the material prepared in a lower generation. The individual lattice structures of each generation can be independently classified by the type of architecture (CC, CA, or iO) and by its material (e.g., polystyrene (PS), poly(methyl methacrylate) (PMMA), SiO_2, TiO_2, Al_2O_3), which for example is described as CA(PS)@iO(SiO_2) for an amorphous colloidal aggregate of PS particles inside a crystalline inverse silica opal.

The hierarchical materials discussed here up to generation 2 were prepared by a simple dip-coating technique. For this purpose, an inverse opal (iO) comprising of micrometer-sized voids was filled with colloids, which were one order of magnitude smaller, and consisted either of polystyrene or silica. This procedure led to the formation of an inverse opal filled with a secondary colloidal phase of smaller periodicity abbreviated as CA(PS)@iO or CA(SiO_2)@iO. The CA(PS)@iO can be backfilled using a sol-gel process, resulting in a double-periodic inverse opal structure (DPiO) after removal of the organic components. The term "double-periodic" refers here to the coexistence of two length scales in the structure provided by the particle dimensions of the large and small templating polymer particles, but does not infer any type and degree of order. An all-silica DPiO can be structurally inverted by infiltration with a polymer. This essentially yields, after silica matrix removal, an opal of two distinct periodicities (one crystalline given by the large host matrix, and one with potentially lower order or even amorphous given by the infiltrated PS or silica spheres), termed double-periodic colloidal aggregate (DPCA). Analogously, the CA(SiO_2)@iO can be backfilled with monomer followed by polymerization. In this case, dissolution of the SiO_2 components results in an inverse opal with small interior periodicity and a large colloidal crystal superstructure (iO@CC). These two- and three-step processes allow the combination of various materials at different length scales, such that novel material properties may be tailored by an appropriate material choice and structural hierarchy. Further levels of structural hierarchy could be added by a top-down micrometer-sized structuring of the iO host[31] or by bottom-up introduction of nanoscopic pores into the 2nd generation iO using self-organizing surfactant or polymer sol-gel formulations.[4]

2. Results and Discussion

The strategy for the fabrication of a whole family of hierarchically structured opaline materials including colloidal assemblies inside an inverse opal (CA@iO), a double-periodic colloidal assembly (DPCA), and a double-periodic inverse opal (DPiO), is outlined in **Figure 1**.

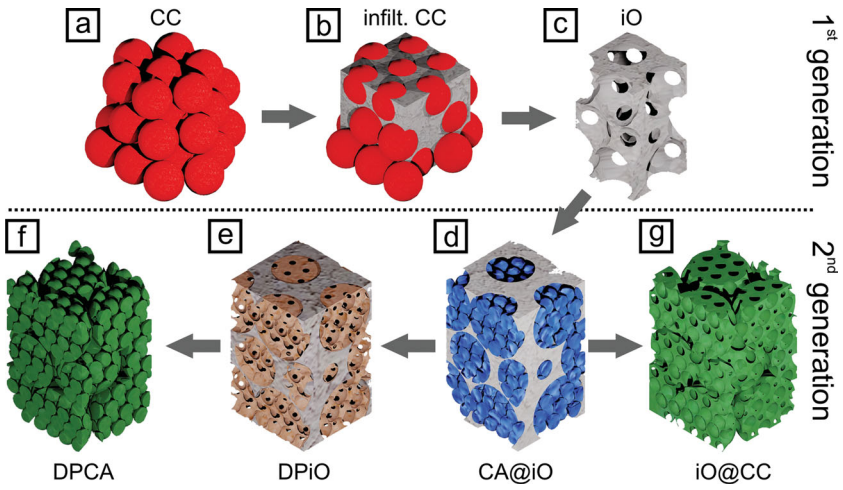

Figure 1. Family tree of hierarchically structured inverse opals and colloidal crystals. a) A colloidal crystal (CC) consisting of 1137 nm polystyrene nanoparticles (red) is prepared by vertical lifting deposition. b) After tempering at elevated temperatures, the CC is infiltrated with inorganic nanoparticles (grey: SiO_2, TiO_2, or Al_2O_3 nanoparticles). c) Pyrolysis removes the polymer template particles and results in the host inverse opal (iO, grey). d) The iO can be backfilled with polystyrene or silica mesoparticles (blue, 90–150 nm), yielding a colloidal aggregate in the host inverse opal matrix (CA@iO). e) Infiltration of the polymeric CA@iO with a sol-gel precursor (brown) and ensuing calcination results in composite materials with the hierarchical structure of a double-periodic inverse opal (DPiO, grey-brown). f) The DPiO can be inverted by monomer infiltration, photopolymerization, and skeleton dissolution, giving a polymeric double-periodic colloidal assembly (DPCA, green). g) By inversion of a CA@iO with a polymer, an inverse opal structured on a colloidal crystal lattice (iO@CC, green) is obtained.

For the fundamental structure motive of a basic fcc lattice, a colloidal crystal constituting of large PS particles (diameter of 1137 nm) was chosen as parent template (Figure 1a, red).

Infiltration of the interstitial volume between the large polymer particles with an inorganic matrix (Figure 1b, grey phase between red spheres) was performed with metal oxide nanoparticles, similar to the procedure of Gu et al.[32], as this approach leads to a minimum shrinkage of the iO during calcination (Figure 1c). Furthermore, this method is very versatile, since in principle any dispersable nanoparticles made of metals, metal oxides, alloys, or mixtures thereof, can be used for infiltration.

In a subsequent vertical lifting step a second colloidal aggregate consisting of smaller colloidal particles (blue spheres in Figure 1d) is deposited inside the free voids of the host matrix iO (leading to a CA@iO). One can fabricate colloidal assemblies of both, polymer (CA(PS)@iO) and silica particles (CA(SiO_2)@iO) inside the first inverse opal.

Depending on the material combination chosen for the CA@iO, in the following process this composite CA@iO can either be infiltrated with monomer and ensuing polymerization, which leads to mesoporous, interconnected polymer particles with an inverse opal architecture arranged in an opaline superstructure (iO@CC, green phase in Figure 1g). Or the CA@iO is infiltrated with a sol-gel formulation of another metal oxide precursor and after pyrolysis of the polymer particle template an inverse opal (brown, Figure 1e) within a larger inverse opal (grey) is obtained, which is termed double-periodic inverse opal (DPiO).

Finally, such DPiO structures can be inverted once more by infiltration with a liquid monomer and photopolymerization, followed by removal of the templating inorganic matrix. Thus, a hierarchical material is obtained, where 3D structured particles with an internal colloidal aggregate architecture are arranged on a colloidal crystal lattice (double-periodic colloidal aggregate, DPCA, Figure 1f).

2.1. Inverse Opals by Infiltration with Nanoparticles

The basic templating colloidal crystal (CC, Figure 1a, red) is prepared in the first fabrication step by vertical lifting deposition and consists of large 1137 nm polystyrene spheres arranged on a fcc lattice. The contact area between adjacent polymer particles in this CC can be increased by annealing at elevated temperatures to soften the polymeric material and induce fusion of the PS particles. This process step allows tailoring the corresponding interconnecting pore size in the inverted opal structures (iO), as they are directly prepared from the annealed CC template (Figure 1c). In turn, the dimensions of the interconnecting pores are important for subsequent filling with mesoscopic particles (e.g., to prepare the CA@iO in Figure 1d). The annealing time of the CC needs to be adjusted to give a maximum diameter of the open pores in the resulting iO, but also to leave large enough ridges (formed by the interstitial space in the CC template) for the inverse opal to form a stable network. The results are summarized in Figure S1 in the Supporting Information. Exposure to low temperatures (93 °C) even for prolonged times (15 min) has a minimum effect on the interconnecting pores, which are about 180 nm in diameter. This temperature is slightly below the T_g of the constituting PS polymer of around 105 °C. For comparison, the diameter of the as-prepared pores obtained by co-deposition of PS and silica nanoparticles was also found to be ≈180 nm. Going to higher temperatures (104 °C) the polymer particles are getting softer and pores of ≈300 nm can be found after 5 to 10 min. Longer annealing times (15 min to 30 min) increase the contact area between neighbouring spheres and thus lead to larger pores of 360 nm (Figure S1c, Supporting Information) and 490 nm (Figure S1d, Supporting Information) between the free voids. This is accompanied by the evolution of macroscopic cracks, which start to form in rectangular blocks in the homogenous crystal film. In each sample, the final diameter of the spherical open voids was found to be 1050–1080 nm, which corresponds to a shrinkage of less than 8% compared to the initial latex particle dimension. As one can deduce from Figure S1d, Supporting Information, a compromise between large pores and a stable host matrix structure has to be established. Too long annealing times or too high temperatures lead to gradual closure of the interconnecting ridges in the inorganic iO. They ultimately become too small to be penetrated by the inorganic nanoparticles, which are used for infiltration (ranging from 5 nm to 30 nm in the cases shown here to form the skeleton iO matrix). Additionally, the probability of clogging increases, which also leads to defects in the replica. As an optimum, a pore diameter of about 400 nm was deduced for the particles used here.

In the next step, a complete infiltration of the interstitial space with inorganic nanoparticles had to be achieved (Figure 1b) by vertical lifting deposition of the annealed CC from the inorganic nanoparticle suspension. For a successful and complete infiltration of the colloidal template, the nanoparticle concentration and the lifting speed of the substrate had to be adjusted. Good results could be obtained with dispersions of 5 wt% to 10 wt% silica nanoparticles and lifting speeds of 1–2 μm s^{-1}. 20 vol% ethanol was added to the dispersion in order to decrease the surface tension and thus facilitate complete infiltration into the free voids of the template. In some regions, an excess layer of silica particles formed on top of the colloidal crystal giving a flat and closed top surface. The evolution of cracks happens inevitably with this method during drying of the dispersion. For samples with no excess layer, block-shaped domains of typically several tens of micrometers in width and a few hundred micrometers in length were found. Usage of higher particle concentrations or lower lifting speeds increased the risk of overlayer formation and ultimately led to disintegration of the template from the supporting substrate by pronounced cracking or curling.[33]

Removal of the constituting polystyrene spheres by pyrolysis in air at 450 °C for several hours yields the inverse opal, which will serve as host structure (iO, Figure 1c) for succeeding process steps. The versatility of the nanoparticle infiltration procedure was further explored with TiO_2 and Al_2O_3 nanoparticles. Dispersions of 10 wt% particle concentration were used in both cases and the lifting speed was set to 2 μm s^{-1}. A comparison of iOs from all three host matrix systems is compiled in **Figure 2** as top and side view scanning electron microscopy (SEM) images.

In Figure 2a,d, the good hexagonal ordering of the SiO_2 iO matrix can be seen. The side view image (Figure 2d) reveals a thin excess layer of silica particles (the measurement was conducted on a delaminated flake of the inverse opal, which is the reason why the excess layer is at the bottom right corner and not on top).

A remarkable difference to the other two nanoparticles is the high filling factor of the SiO_2 matrix. Whereas the SiO_2 nanoparticles completely fill the free space, open parts, and merely just a covering of the polymer particles interface was observed in the other two cases after calcination. This difference in infiltration was already pointed out by Zakhidov et al.,[13,34] who differentiated between volume-templating and surface-templating. The surface-templating behavior of the TiO_2 and Al_2O_3 nanoparticles may best be seen in Figure 2b,f. In the first case the thin shells, which wrap around the particles are clearly seen; in the second case the inverse opal looks like being constituted of hollow Al_2O_3 shells.

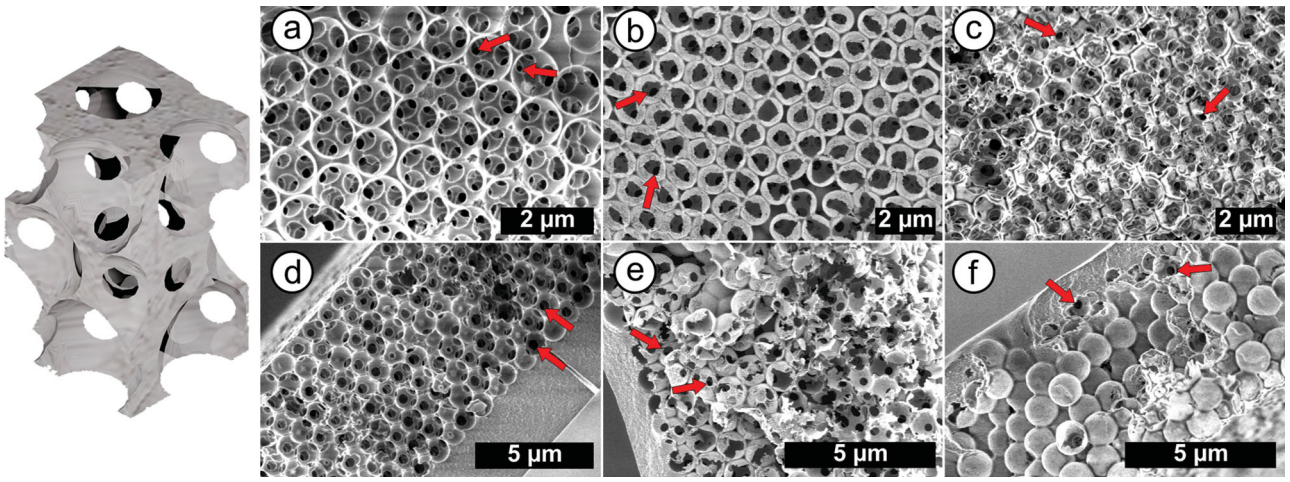

Figure 2. a–c) Top view and d–f) side view SEM images of inverse opal host matrices (iO) consisting of different materials. a,d) SiO_2, b,e) TiO_2 (anatas), and c,f) Al_2O_3 (γ-aluminium oxide). Red arrows emphasize the open cell structure of the inverse opal host.

Due to the thin walls of the resulting host matrix, the inverse opals constituting of TiO_2 and Al_2O_3 are expected to be more fragile compared to their SiO_2 analogue. Nevertheless, they also replicate the template structure with only a minimum of shrinkage. An 18% size reduction was measured for the TiO_2 matrix, and 7% for the Al_2O_3 case.

Nanoparticle infiltration into a colloidal crystal template is dominated by capillary and drag forces as the particle suspension infuses into the interstitial space to drag nanoparticles with it and immobilize the spheres within the polymer template. Thus, the free volume is continuously filled as drying of the dispersion proceeds. In case of repulsive forces between the polymer particle host and the inorganic nanoparticles, with appropriate nanoparticle concentration and drying time, this situation is expected to result in volume-templated composites. The presence of surface-templated structures as obtained by TiO_2 and Al_2O_3 nanoparticles, hints towards an additional attractive interaction between the polymer surface and the inorganic nanoparticles. Attractive forces will result in immobilization of nanoparticles on the polymer spheres, and in particular in the tiny interconnecting channels it will hamper the diffusion of further nanoparticles to the drying front. Therefore, even in the case of appropriately concentrated nanoparticle suspensions, a complete volume templating cannot be achieved anymore, and surface-templated structures will be obtained. In such a scenario, the particle size and size distribution will also play an important role, as this will strongly impact the tendency to block the interconnecting pores. For the nanoparticles used in our case, both size and size distribution were larger for TiO_2 (5–30 nm) and Al_2O_3 (10 ± 5 nm), compared to SiO_2 (≈7 nm), making it more likely to result in surface-templating.

2.2. Infiltration of Colloidal Particles into Inverse Opals

The next level of complexity in the hierarchical order is reached by infiltration of the iO host matrix with another set of colloidal particles (compare Figure 1c). Clearly, the particles, which can possibly be used for filling the free voids of the inverse opal, have to be smaller than the interconnecting pores. A systematic study on the filling efficiency in dependence on the particle diameter was conducted; representative results for various CA@iO systems are given by top view and side view SEM images in **Figure 3**.

The experimental results document that all particles with diameters from 93–220 nm infiltrate into the SiO_2 host inverse opal. However, a complete filling of the free voids is only achieved with particles of 130 nm in diameter or smaller. This corresponds roughly to a third of the pore diameter. A complete filling of the host matrix is mandatory in order to obtain a second continuous network after the next replication step (Figure 1e,g). However, this is not only dependent on the particle size, but can also be influenced by the particle concentration and lifting speed, analogous to the nanoparticle infiltration step. Furthermore, these parameters need to be adjusted such that complete filling of the iO host is achieved, depending on the thickness of the open cell skeleton. Concomitantly, an over-infiltration of the inverse host, that is, the formation of a colloidal crystal overlayer of the mesoparticles, should be avoided. Using particle concentrations of 0.25 wt% and 0.50 wt% for PS latex and 2.5 wt% for silica spheres in combination with a rather low withdrawal rate (400 nm s^{-1}), we were able to achieve complete filling of the SiO_2 iO host, as long as the particles were smaller than 1/3 of the interconnecting pore diameter. One has to bear in mind that by using vertical lifting deposition, the drying front of the colloidal dispersion proceeds in a perpendicular fashion through the iO host matrix. Thereby, ample time and a continuous particle supply are provided to fill the porous layer. The main driving forces here are capillary forces, which fill the matrix with dispersion, convective forces, which drag PS and silica particles to the drying front, and capillary attraction between the metaloxide matrix walls and among the particles, which lead to aggregation and volume filling of the porous voids. Due to defect sites in the host material and

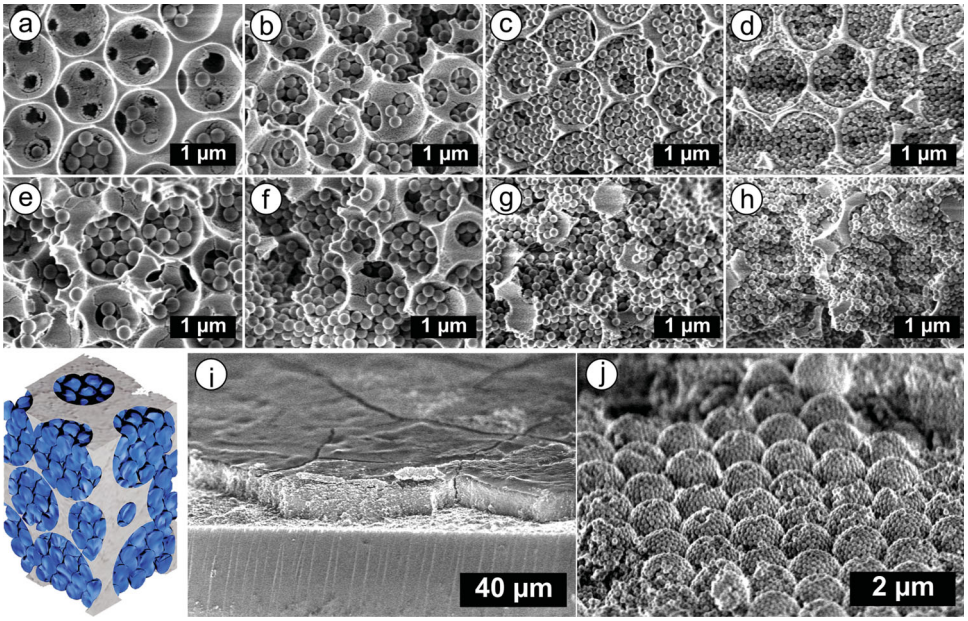

Figure 3. Different CA@iO structures prepared by infiltration of a host inverse SiO_2 opal with PS particles of varying diameters: a,e) 220 nm, b,f) 180 nm, c,g) 130 nm, and d,h) 93 nm. All dispersions were adjusted to 0.25 wt% PS particle concentration. Top row shows top view and bottom row side view SEM images. The host inverse opal had spherical voids of about 1 µm and pore diameters ranging from 380 nm to 470 nm. i) Side-view image of a large area of an inverse opal infiltrated with polystyrene mesoparticles (CA@iO). j) Side-view of a sectioned area. The 93 nm PS particles self-assemble in a spherically shaped geometry imposed by the inverse opal host.

an increased material roughness, meniscus pinning can occur, which results in undesired material deposition on top of the host opal at some regions.

An optimized example of a fully infiltrated inverse opal is shown in Figure 3. In this case 93 nm PS spheres were used. The host matrix is completely filled from top to bottom without the formation of an excess layer. The complete filling is corroborated in Figure 3j by the hierarchical arrangement of the PS mesoparticles within the voids of the inorganic iO template. One finds that the shape of the PS mesoparticle lattice perfectly adapts to the structure of spherical void of the iO template and that the colloids readily arrange in a close-packed geometry. Apparently, the hexagonal order improves with decreasing particle diameter, as those smaller particles are expected to more easily accommodate the stress imposed by the confining geometry of the iO template. Here, the key geometry parameters are particle radius versus void radius. On the one hand, an integer multiple of the iO void dimension with respect to the mesoparticle diameter is optimal for a commensurate packing, as reported for graphoepitaxy in other packing geometries.[35] On the other hand, a smaller radius of curvature in the iO void with respect to the mesoparticle size (in essence a larger void) will lead to a smaller distortion of the crystal lattice in the mesoparticle CC within the spherical void.

Infiltration of TiO_2 and Al_2O_3 inverse opals was conducted in the same way. The ordered porous network was mainly maintained during this step, even though the matrix constituted of thinner ridges, as pointed out above. The filling was not as complete and homogenous as in the SiO_2 case. Especially regions with singly adsorbed particles were found in the TiO_2 case (Supporting Information, Figure S2). This behavior is similar to the surface-templating of the TiO_2 nanoparticles onto the PS template as seen in Figure 2. A potential reason could be a stronger attraction of the PS mesoparticles to the surface of the TiO_2 iO by the sulphate groups on the PS particles from the initiator, which would reduce the mesoparticle mobility inside the inorganic iO template and thus hamper optimal packing. Concomitantly, PS particles adsorbed at or close to the interconnecting pores can prevent further particles to diffuse into the free voids, leading to incomplete filling. The use of small enough mesospheres would be less affected by such an adsorbed layer and could result in completely filled voids. Another factor limiting the filling efficiency becomes apparent from Figure S2, Supporting Information. The presence of a metaloxide overlayer or closed facet of the inverse opal lattice severely reduces the evaporation rate during the polymer dispersion infiltration step and consequently reduces convective assembly.

The range of materials can be broadened even further by the use of SiO_2 colloidal particles instead of PS latex. The results are given in Figure S3 in the Supporting Information, where a complete infiltration of a SiO_2 template with silica mesoparticles is shown.

2.3. DPiO Comprising of Various Materials

CA@iO from inverse opals, which were backfilled with PS particles, can be infiltrated with a sol-gel solution containing the desired metal oxide precursor in order to yield a secondary inverse opal structure after PS particle pyrolysis (DPiO, Figure 1e). A simple procedure to obtain a

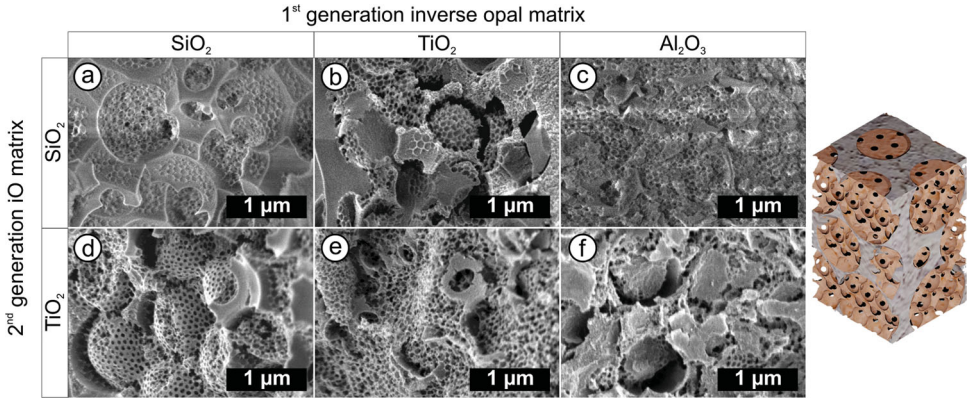

Figure 4. SEM images of a family of different composite DPiO. The top row is composed of SiO_2 as the mesoporous matrix filling, the bottom row consists of TiO_2. The corresponding macroporous host iO material is indicated on top of each column.

nanoparticle-infiltrated colloidal crystal utilizes co-deposition of the polymer colloids and inorganic nanoparticles. Due to the small mesoparticle sizes (93 nm) employed here for the secondary colloidal crystal (CA(PS)@iO), a co-deposition of PS mesoparticles and metaloxide nanoparticles is not feasible for the host matrix filling, as the metal oxide nanoparticles are too large to effectively fit into the free voids of the mesoparticle lattice. Instead, two types of sol-gel precursors were chosen, tetraethyl orthosilicate (TEOS) and titanium(IV) ethoxide. Combining these two materials with all three primary iO matrices (SiO_2, TiO_2, and Al_2O_3) yielded six macro- and mesoporous composite materials (DPiO), shown in **Figure 4**.

In all cases, the structural DPiO hierarchy of tiny mesoporous networks being embedded in the larger host iO matrix can be identified. It shall be pointed out that the void size is around 100 nm, given by the templating PS mesospheres and the interconnecting pores fall in the mesoporous range. Material combinations of SiO_2, TiO_2, and Al_2O_3, as primary host iO matrix with SiO_2 and TiO_2 as secondary iO structure, are demonstrated here. However, the method is not limited to these compounds, but any combination of metal oxide nanoparticles (for the primary iO) and sol-gel precursor (for the secondary iO) should be accessible. The presence of the different elements in the DPiO was confirmed by EDX measurements and their relative ratios are listed in **Table 1**. A comparison of the relative element ratios experimentally determined and theoretically expected is given in **Table 2**.

Table 2. Comparison of measured and theoretical relative element ratios in completely filled composite DPiO (material of the small second generation iO @ large first generation host iO). The theoretical values are given in brackets.

relative ratio [%]	TiO_2@SiO_2	SiO_2@TiO_2	SiO_2@Al_2O_3	TiO_2@Al_2O_3
Si	61.8 (45.8)	63.7 (31.1)	53.3 (25.1)	
Ti	38.2 (54.2)	34.4 (68.9)		65.2 (35.2)
Al			46.8 (74.9)	34.8 (64.8)

The energy dispersive X-ray (EDX) measurements evidence the presence of all individual elements as expected. Only a semi-quantitative analysis was conducted, since the atomic ratios already mismatch for the pure SiO_2 case by about 5%. When comparing the expected element ratios to the experimental results (Table 2), one finds that in all cases a significantly lower amount of Ti and Al was incorporated compared to Si. This corroborates the earlier finding of surface templating of TiO_2 and Al_2O_3 nanoparticles in the formation of the host opal. The thin shell obtained from TiO_2 and Al_2O_3 nanoparticle infiltration does not efficiently fill the free space between the templating PS particles and therefore leads to the deposition of less material than expected. In contrast, SiO_2 replicates the full volume, leading to higher relative elemental ratios. In the case of TiO_2@Al_2O_3 DPiO, a higher Ti content was observed. Here, using a sol-gel rather than nanoparticles for the impregnation

Table 1. Total element ratios in the composite DPiO as determined by EDX measurements (material of the small second generation iO @ large first generation host iO).

atomic [%][a)]	SiO_2@SiO_2[b)]	TiO_2@SiO_2[b)]	SiO_2@TiO_2[b)]	TiO_2@TiO_2[b)]	SiO_2@Al_2O_3[c)]	TiO_2@Al_2O_3[b)]
Ti L	–	9.7	7.6	18.8	–	8.8
Ti K	–	14.0	18.1	32.7	–	29.2
Si K	38.4	22.7	31.7	–	21.3	–
Al K	–	–	–	–	18.7	15.6
O K	61.6	53.6	42.6	48.5	60.0	46.4

[a)]L and K denote the respective atomic orbitals; [b)]Measured with 20 kV; [c)] Measured with 10 kV.

of the CA(PS)@iO with TiO_2, leads to a more complete filling of the interstitial free space compared to the surface templating of the Al_2O_3 nanoparticles of the iO host.

An efficient and complete filling of the template structure with the sol-gel solution is crucial for the successful replication of the hierarchical structure. Shrinkage during calcination can contribute to deviations from the expected element ratio as determined by EDX. The effect of shrinkage can be seen in SEM images in Figure 4b,d, where voids were incompletely replicated. Macroporous iO spheres, which are embedded inside the larger host iO voids, are discernible but due to the shrinkage they do not completely fill the larger inverse opal structure after calcination. The opaline structure is better maintained in the case of the SiO_2 network. The surface-templating of the TiO_2 and Al_2O_3 nanoparticles is prone to cracks after sol-gel infiltration and the second calcination step. Additionally, the necessity to fracture the DPiO for examination by SEM can introduce further defect artefacts.

2.4. Replication with a Polymer Matrix, DPCA and iO@CC

After fabricating all SiO_2 hierarchical DPiO material, the final structure can be replicated by polymerization of a monomer inside the template; here, methylmethacrylate (MMA) was specifically utilized. The SiO_2 DPiO template can be gently removed after replication by treatment with diluted hydrofluoric acid (HF). We demonstrate access to two types of structures with this method. The first strategy employs an all-SiO_2 DPiO (Figure 1e) and yields a double-periodic colloidal assembly (DPCA) consisting of micrometer-sized spheres with an interconnected sub-100 nm particle fine structure (Figure 1f, **Figure 5**a). The second route uses an inverse opal, which has been backfilled by mesoscopic silica particles (CA(PS)@iO). This hierarchical structure replicates into a network of micrometer-sized PMMA particles with an inverse opal interior structure of sub-100 nm voids and pores, termed iO@CC (Figure 1g,5b).

The successful formation of two types of hierarchically structured PMMA scaffolds can be seen in Figure 5. The resulting structures show complimentary architectures as one consists of a PMMA nanoparticle superstructure as double-periodic colloidal assembly (DPCA, Figure 5a), whereas the other system contains micrometer-sized spheres with an inverse opaline interior structure (iO@CC, Figure 5b). Unfortunately, the SEM images appear slightly blurred due to partial PMMA degradation by the electron beam. This degradation process induces an immediate collapse of the fine structures and leads to a featureless, continuous film. Thus, the pictures had to be taken with low integration times and at low acceleration voltages.

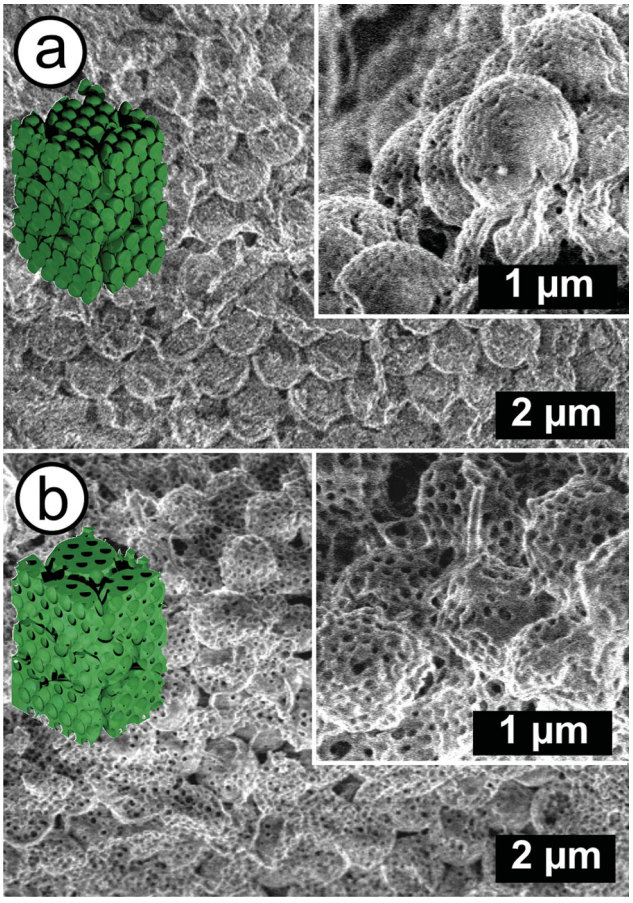

Figure 5. a) Hierarchical DPCA of PMMA particles consisting of interconnected spheres which was templated by a silica DPiO (compare Figure 1e). b) Hierarchical PMMA iO@CC structure consisting of interconnected voids and pores, which were templated by 130 nm SiO_2 particles in a silica host matrix (CA(PS)@iO) (compare Figure 1d).

3. Conclusions

A methodology was presented to structure porous inverse opals on two length scales, these being 1 micrometer and 30–100 nm in size. The repeated infiltration of a colloidal crystal and its replica by vertical lifting deposition yielded hierarchical composite materials with combinations of SiO_2, TiO_2, and Al_2O_3 phases. The filling fraction had to be controlled in each step in order to avoid the deposition of an excess material layer on top of the template film. Mesoparticles with dimensions of up to a third of the pore diameter effectively filled the voids and introduced a second level of structural hierarchy. However, void filling was not only a matter of geometric constraints, but also the involved materials played a crucial role. Predominant surface-templating of TiO_2 and Al_2O_3 nanoparticles hints to an attractive interaction with the polymer template, whereas the SiO_2 particles were found to infiltrate the entire volume. The hierarchical architecture of all-silica materials could be inverted with a polymer replica, resulting in micrometer-sized spheres either composed of PMMA mesoparticle aggregatess or air-holes with iO geometry corralled by PMMA. Whereas further development needs to be directed towards the large-scale homogeneity of the porous composite material, the clear potential of this methodology lies in its versatility and simplicity. As demonstrated, a large range of material classes from inorganic compounds to organic polymers can be employed. Such hierarchically structured materials can find applications in technologies requiring a large surface area, such as dye sensitized solar cells, as demonstrated by Cho et al.[27]

4. Experimental Section

Colloidal Crystal Fabrication and Annealing: 1137 nm PS colloidal particles were synthesized according to Ottewill[36] and used to fabricate colloidal crystals, which served as template for the inverse opals. The colloidal crystals (CC) were prepared by vertical lifting deposition of a 2 wt% aqueous dispersion of the PS particles onto plasma cleaned glass slides at a speed of 600 nm s^{-1} (Figure 1a).[37,38] Temperature and humidity were set to 20 °C and 50%, respectively. The colloidal templates were annealed in a Heraeus vacuum oven with the temperature set to 115 °C, which corresponded to a temperature of 104 °C at the sample position. In order to compensate for the limited temperature control among different experiments, the annealing time was adjusted between 15 min and 25 min. The evolution of tiny cracks in the homogenous colloidal crystal was taken as an indication of the onset of particle fusion.

Infiltration with Metal Oxide Nanoparticles for Inverse Opal Structure Fabrication: Three different metal oxide nanoparticle dispersions were used for infiltration of the annealed colloidal crystals (infilt. CC) yielding the host inverse opal (iO) (Figure 1b,c).[32] In most cases, a 5 wt% aqueous dispersion of LUDOX SM silica nanoparticles (SigmaAldrich, 7 nm diameter), a 10 wt% aqueous dispersion of TiO_2 nanoparticles (NanoAmor, 5–30 nm, Anatas), and a 10 wt% aqueous dispersion of γ-Al_2O_3 nanoparticles (NanoAmor, 10 nm) was used. The nanoparticle dispersion was mixed with EtOH p.a. in a 8:2 (nanoparticle suspension:EtOH) volume ratio. Subsequently, the template colloidal crystal was immersed in the nanoparticle dispersion and slowly withdrawn at room temperature and humidity ranging from 30%–60%. The withdrawal speed was set to 1 or 2 µm s^{-1}. The PS template was pyrolized in air at 450 °C for several hours to yield the inorganic host inverse opal. A fast heating rate (≈10 K min^{-1}) was applied.

Infiltration with Polymer and Silica Colloids (CA(PS)@iO and CA(SiO2)@iO): Infiltration of the host inverse opal was conducted with aqueous dispersions of PS and silica colloids by vertical lifting deposition (Figure 1d). PS dispersions, synthesized according to Ottewill,[36] were used at a concentration of 0.25 wt% (220 nm, 180 nm, 130 nm), or 0.5 wt% (93 nm), and stirred silica dispersions, synthesized according to Giesche,[39–41] were used at 2.5 wt% (130 nm). The deposition speed was in all cases 400 nm s^{-1} at 20 °C and 50% RH.

Sol-Gel Infiltration and Photopolymerization (DPiO, DPCA, and iO@CC): The samples, which had been loaded before with PS particles into the host inverse opal (CA(PS)@iO), were infiltrated with a sol-gel precursor solution of the desired final metal oxide in order to generate the second inverse opal matrix. For a silica matrix a sol-gel precursor consisting of TEOS (2 mL, Aldrich, >99%), EtOH (2 mL), and HCl (0.1 mL) was dropped several times onto an inclined sample after 10 min of prehydrolysis. The substrate was left standing upright in the sol-gel solution for 45 min. Infiltration with TiO_2 was conducted by placing the substrates upright in a vial containing a titanium ethoxide (Aldrich, 75%, used as received) solution, which was diluted 3:1 with EtOH. A few drops of the sol-gel precursor were dropped onto the sample. Condensation was allowed for 30 min. Finally the PS template was removed by calcination at 450 °C in air to yield a double-periodic inverse opal (DPiO, Figure 1e). The samples, which were infiltrated with colloidal silica particles ($CA(SiO_2)$@iO), were subjected to photopolymerization of MMA. A 15 wt% solution of Irgacure 907 in MMA was dropped several times onto the substrate and UV polymerized using a UV LED (365 nm, ≈1.74 mW cm^{-2}) for 5 min. This procedure was repeated several times until a clear, yellowish film was obtained. The same procedure was applied to a DPiO only consisting of SiO_2 matrices. In either case, the silica was removed by etching with hydrofluoric acid (HF). The samples were immersed for about 2 min into a 4 vol% solution of HF and rinsed twice with MQ water resulting either in a double-periodic colloidal assembly (DPCA, Figure 1f) or inverse opal with a colloidal crystal superstructure (iO@CC, Figure 1g).

Characterization: SEM images (LEO Gemini 1530, Zeiss) were taken on flakes of the film, which were scratched off the supporting substrate with a scalpel. EDX measurements were conducted on a FEI Nova 600 Nanolab.

Supporting Information

Supporting Information is available from the Wiley Online Library or from the author.

Acknowledgements

The authors thank Prof. Mukundan Thelakkat and Werner Reichstein (University of Bayreuth) for assistance with SEM measurements. Maren Müller is acknowledged for the EDX analysis. M.R. thanks the VCI for financial support. The experiments were partially performed at the Max Planck Institute for Polymer Research, Mainz, Germany.

Received: March 4, 2013
Revised: April 15, 2013
Published online: May 31, 2013

[1] Y. J. Lee, P. V. Braun, *Adv. Mater.* **2003**, *15*, 563.
[2] I. B. Burgess, L. Mishchenko, B. D. Hatton, M. Kolle, M. Lončar, J. Aizenberg, *J. Am. Chem. Soc.* **2011**, *133*, 12430.
[3] S. A. Rinne, F. Garcia-Santamaria, P. V. Braun, *Nat. Photonics* **2008**, *2*, 52.
[4] M. Antonietti, B. Berton, C. Goltner, H. P. Hentze, *Adv. Mater.* **1998**, *10*, 154.
[5] R. Raccis, A. Nikoubashman, M. Retsch, U. Jonas, K. Koynov, H.-J. Butt, C. N. Likos, G. Fytas, *ACS Nano* **2011**, *5*, 4607.
[6] C. M. A. Parlett, K. Wilson, A. F. Lee, *Chem. Soc. Rev.* **2013**.
[7] Y. Li, Z.-Y. Fu, B.-L. Su, *Adv. Mater.* **2012**, *22*, 4634.
[8] F. Yan, A. Ding, M. Gironès, R. G. H. Lammertink, M. Wessling, L. Börger, K. Vilsmeier, W. A. Goedel, *Adv. Mater.* **2012**, *24*, 1551.
[9] Q. Li, M. Retsch, J. Wang, W. Knoll, U. Jonas, *Top. Curr. Chem.* **2009**, *287*, 135.
[10] A. Stein, F. Li, N. R. Denny, *Chem. Mater.* **2008**, *20*, 649.
[11] B. T. Holland, C. F. Blanford, T. Do, A. Stein, *Chem. Mater.* **1999**, *11*, 795.
[12] O. D. Velev, E. W. Kaler, *Adv. Mater.* **2000**, *12*, 531.
[13] A. Stein, *Microporous Mesoporous Mater.* **2001**, *44*, 227.
[14] P. D. Yang, T. Deng, D. Y. Zhao, P. Y. Feng, D. Pine, B. F. Chmelka, G. M. Whitesides, G. D. Stucky, *Science* **1998**, *282*, 2244.
[15] S. Fujita, H. Nakano, M. Ishii, H. Nakamura, S. Inagaki, *Microporous Mesoporous Mater.* **2006**, *96*, 205.
[16] J. Wijnhoven, W. L. Vos, *Science* **1998**, *281*, 802.
[17] B. Gates, Y. D. Yin, Y. N. Xia, *Chem. Mater.* **1999**, *11*, 2827.
[18] K. Burkert, T. Neumann, J. J. Wang, U. Jonas, W. Knoll, H. Ottleben, *Langmuir* **2007**, *23*, 3478.
[19] W. M. Lee, S. A. Pruzinsky, P. V. Braun, *Adv. Mater.* **2002**, *14*, 271.
[20] T. A. Taton, D. J. Norris, *Nature* **2002**, *416*, 685.
[21] M. Muller, R. Zentel, T. Maka, S. G. Romanov, C. M. S. Torres, *Chem. Mater.* **2000**, *12*, 2508.
[22] J. Wang, S. Ahl, Q. Li, M. Kreiter, T. Neumann, K. Burkert, W. Knoll, U. Jonas, *J. Mater. Chem.* **2008**, *18*, 981.
[23] J. Wang, Q. Li, W. Knoll, U. Jonas, *J. Am. Chem. Soc.* **2006**, *128*, 15606.
[24] G. S. Chai, I. S. Shin, J. S. Yu, *Adv. Mater.* **2004**, *16*, 2057.
[25] S. M. Yang, N. Coombs, G. A. Ozin, *Adv. Mater.* **2000**, *12*, 1940.
[26] C.-Y. Cho, J. H. Moon, *Adv. Mater.* **2011**, *23*, 2971.
[27] C.-Y. Cho, J. H. Moon, *Langmuir* **2012**, *28*, 9372.
[28] A. R. Studart, J. Studer, L. Xu, K. Yoon, H. C. Shum, D. A. Weitz, *Langmuir* **2010**, *27*, 955.
[29] N. Vogel, L. de Viguerie, U. Jonas, C. K. Weiss, K. Landfester, *Adv. Funct. Mater.* **2011**, *21*, 3064.
[30] N. Vogel, S. Goerres, K. Landfester, C. K. Weiss, *Macromol. Chem. Phys.* **2011**, *212*, 1719.

[31] B. Hatton, L. Mishchenko, S. Davis, K. H. Sandhage, J. Aizenberg, *Proc. Natl. Acad. Soc. USA* **2010**, *107*, 10354.
[32] Z. Z. Gu, S. Kubo, A. Fujishima, O. Sato, *Appl. Phys. A: Mater. Sci. Process.* **2002**, *74*, 127.
[33] E. Vekris, G. A. Ozin, V. Kitaev, *Adv. Mater.* **2006**, *18*, 2481.
[34] A. A. Zakhidov, R. H. Baughman, Z. Iqbal, C. X. Cui, I. Khayrullin, S. O. Dantas, I. Marti, V. G. Ralchenko, *Science* **1998**, *282*, 897.
[35] A. vanBlaaderen, R. Ruel, P. Wiltzius, *Nature* **1997**, *385*, 321.
[36] J. W. Goodwin, J. Hearn, C. C. Ho, R. H. Ottewill, *Colloid. Polym. Sci.* **1974**, *252*, 464.
[37] C. A. Fustin, G. Glasser, H. W. Spiess, U. Jonas, *Adv. Mater.* **2003**, *15*, 1025.
[38] A. S. Dimitrov, K. Nagayama, *Langmuir* **1996**, *12*, 1303.
[39] H. Giesche, *J. Eur. Ceram. Soc.* **1994**, *14*, 205.
[40] H. Giesche, *J. Eur. Ceram. Soc.* **1994**, *14*, 189.
[41] W. Stöber, A. Fink, E. Bohn, *J. Colloid Interface Sci.* **1968**, *26*, 62.